Highly Sensitive Pressure Measurement based on Multimode Fiber Tip Fabry-Perot Cavity

Wei Ping Chen* and Dongning Wang

College of Optical and Electronic Technology, China Jiliang University, Hangzhou, China

Keywords: Fabry-Perot Interferometer, Multimode Fiber, Pressure Sensors.

Abstract: In this work, a highly sensitive pressure measurement device based on multimode fiber filled with ultraviolet adhesive is presented. The experimental results show that the device has a high gas pressure sensitivity of -40.94nm/MPa, a large temperature sensitivity of 213 pm/°C within the range from 55 to 85°C, and a relatively temperature cross-sensitivity is 5.2kPa/°C. The fiber device is miniature, robust and low cost, in a reflection mode of operation, and has high potential in monitoring environment of high pressure.

1 INTRODUCTION

A variety of Fabry–Perot interferometric sensors based on optical fiber have recently been studied and applied in various industrial areas to measure temperature, refractive index, strain, pressure, and fluid dynamics (Roriz P., et al., 2013. Optical fiber FP interferometer (FPI) pressure sensors can be divided into two types: operated on cavity length change (Pevec S. and Donlagic D., 2012; Guo F et al., 2012; Xu F., et al., 2012; Ma J., et al., 2012; Jin L., et al., 2013; Eom J., et al., 2015; Ran Z., et al., 2015; Hou M., et al., 2014.) or mainly rely on cavity refractive index (RI) variation (Yuan W., et al., 2011; Coelho L., et al., 2012; Hu G., Chen D., 2012; Liu Z., et al., 2012; Wu C., et al., 2010). Many FPI sensors worked on cavity length variation possess relatively low pressure sensitivity compared with those based on thin diaphragm. However, the diaphragm based FPI sensors have a small measurement range, typically a few tens of kPa (Xu F., et al., 2012; Ma J., et al., 2012) and relatively poor mechanical strength. Although the FPI sensors worked on cavity RI change usually have a large measurement range and good robustness, their pressure sensitivity is relatively low, typically on the order of tens of pm/MPa (Coelho L., et al., 2012; Hu G., Chen D., 2012; Liu Z., et al., 2012, Wu C., et al., 2010), except sensor head with a carefully designed (Xu B., et al., 2015), which increases system complexity and manufacturing difficulty.

In this work, a novel fiber tip FPI pressure sensor based on etched end of multimode fiber (MMF) filled with ultra-violet (UV) adhesive is experimentally demonstrated. The fiber tip FP cavity is compact in size, robust in structure, simple in manufacturing, and convenient in operation. Because of the special design of the sensing head, the proposed sensor is effectively exhibits high gas pressure sensitivity of -40.94nm/MPa within the measurement range between 0 and 1 MPa (limited by the pressure meter we used). On the other hand, the device can measure temperature and the refractive index, and their sensitivities are 213 pm/°C within the range from 55 to 85°C, ~-73.54 nm/RIU (RI unit) within the range from 1.332 to 1.372, respectively, which shows its versatile measurement capability. Moreover the fiber tip FP cavity possesses a relatively low temperature cross-sensitivity of 5.2 kPa/°C.

2 DEVICE FABRICATION AND OPERATION PRINCIPLE

The optical fiber FP cavity sensor head is fabricated by an etched MMF filled with UV adhesive. During the fabrication process, the end face of MMF with a core diameter of 62.5 μm and a nominal effective RI of 1.4682 (at 1550 nm) is etched by use of hydrofluoric (HF) acid to form a tapered hole cavity. The UV adhesive (Norland, NOA68) employed can

147

sustain the temperature change from -80°C to 90°C, and has the RI of 1.54. The steps of fabrication are illustrated in Fig. 1.

a) Firstly, a section of MMF is etched for ~10 minutes by use of HF acid with the concentration of 40% before a taper-shaped hole of several tens micrometers in depth is formed at the end face of the MMF.

b) Secondly, the taper-shaped hole created is filled with UV adhesive. As shown in the figure, an inner air-cavity is formed inside the UV adhesive due to the remaining air in the taper-shaped hole region during the process of UV adhesive filling. Then, employing the UV light to solidify the UV adhesive.

The two reflection surfaces of R_1 and R_2 create an FP cavity (C_1). The light lunched into the inner air-cavity is split into three beams: one traveling along the MMF arrives at R1, part of the light is reflected back which is denoted by I1, and the rest continues to propagate until reaching R_2 and experiencing partial reflection, denoted by I_2. The light beam transmitted through R_2 finally arrives at R_3 and is partially reflected again which is denoted by I_3. The two reflection surfaces of R_2 and R_3 thus forming another FP cavity (C_2). Meanwhile, the two reflection surfaces R_1 and R_3 can also form an FP cavity (C_3) with a cavity length that is equal to the sum of cavity lengths of C_1 and C_2. The cavity lengths for C_1 and C_2 are ~37.7 and ~18.7 μm, respectively.

Fig. 3(a) displays the reflection spectrum of the device sample fabricated. And the fiber tip FPI sensor corresponding spatial frequency spectrum obtained by use of fast Fourier transform as shown in Fig. 3(b), there are two dominant side peaks in the spatial frequency spectrum, located at ~0.0239 and ~0.0563 nm^{-1}, respectively, which indicates an interference pattern of two FP cavities.

The well-known expression of free spectral range (FSR) is written as

$$FSR = \lambda^2/2nL \quad (1)$$

where λ is the wavelength, n is the RI of the cavity, and L is the cavity length. As the RI of UV adhesive is 1.54 and the cavity lengths of C_1 and C_2 are ~37.7 μm, ~18.7 μm, respectively, by taking the wavelength of 1550 nm, the spatial frequency peak positions for three FP cavities C_1, C_2 and C_3 can be determined as ~0.0314, ~0.0239 and ~0.0554 nm-1, respectively. This reveals that C_2 and C_3 are the dominant FP cavities as the experimentally obtained

results agree well with those obtained from the calculations. Thus, the output spectrum of the device consists of two superimposed FP spectra of C_2 and C_3.

The reflection intensity (I) of the MZI can be expressed by three beam interference theory as

$$I=I_1+I_2+2I_3+2\sqrt{I_2I_3}\cos\Phi_{23}+2\sqrt{I_1I_3}\cos\Phi_{13} \quad (2)$$

where I_1, I_2, and I_3 are the light intensity reflected from adhesive-air surface R_1, air-adhesive surface R_2, and adhesive-air surface R_3, respectively, and Φ_{23} and Φ_{13} are the introduced phase shifts of the cavity C_2 and C_3 , respectively, given by

$$\Phi_{23} = \frac{4\pi n_2 L_2}{\lambda} \quad (3)$$

$$\Phi_{13} = \frac{4\pi(n_1 L_1 + n_2 L_2)}{\lambda} \quad (4)$$

where n_1 and n_2 are the RI of air, UV adhesive, L_1 and L_2 are cavity length of C_1 and C_2, respectively.

From Eqns. (2) - (4), by taking n_1=1, n_2=1.54, the cavity lengths L_1=37.7 μm, L_2=18.7 μm, and the reflection coefficient of the surface of R_1, R_2 and R_3 as $(n_1-n_2)^2/(n_1+n_2)^2$=0.0452, the reflection spectrum of the FP cavity device can be simulated and the result obtained is displayed in Fig. 4, together with that obtained from the experiment as shown previously in Fig, 3(a), to facilitate the comparison. It can be seen from Fig. 4 that the two reflection spectra have nearly the same waveform, and their intensity difference comes from the insertion loss of the device while the wavelength shift existed in the experimental fringe pattern is likely due to the initial phase of the fringe pattern and the dispersion effect of the optical fiber.

3 EXPERIMENTAL RESULTS AND DISCUSSION

Fig. 5 shows the schematic of the experimental setup used to test the response of FP sensor head to gas pressure. A broadband source (BBS) centered at 1550 nm is used to illuminate the FPI through a circulator. The reflection spectrum of the FPI is observed by an optical spectrum analyzer (OSA) with the resolution of 0.05 nm to monitor the spectrum. The sensor head is placed in a gas chamber, where the gas pressure can be adjusted by use of an air pump (Wisdom Billiton, Y039), measured by a pressure meter (ZHITUO, YB-150). The sensor output is directed to an optical spectrum

analyzer (OSA) with the resolution of 0.05 nm to monitor the spectrum.

We investigated the responses of the fiber tip FPI pressure sensor samples with different pressure. In the measurement, the fiber in the chamber was kept in a straight line to avoid any bending-induced effects, gradually increasing the pressure from 0.02 to 0.04 and then to 0.92 MPa with a step of 0.04 MPa, and the reflection spectrum was monitored in real-time by use of an OSA. Fig. 6 and its inset demonstrate the shift of dip wavelength in the reflection spectrum with the pressure variation. It can be seen from the figure that the dip wavelength is decreased with the increase of pressure, and a linear response with a sensitivity of -40.94nm/MPa is obtained in the range of 0.02 to 0.92 MPa.

The high temperature sensing capability of the device are tested by placing the sensor head in an electrical oven and gradually increasing the temperature from room temperature to 85°C with a step of 5°C. During the experiment, to make sure the temperature was stabilized in the chamber, the temperature was stayed for 10 minute at each step. Fig. 7 presents the dip wavelength variation with the temperature change and its inset demonstrates the reflection spectra at different temperatures. A fringe dip near ~1540 nm at the temperature of 30°C is found to experience a red shift with the increase of temperature. The highest sensitivity obtained is ~213 pm/°C within the temperature range from 55°C to 85°C. However, considering of the pressure sensitivity of -40.94nm/MPa obtained in the experiment, the temperature cross-sensitivity is calculated to be only 5.2 kPa/°C, which is much smaller than that of the sensors based on side-hole dual-core PCF (Hu G. and Chen D., 2012) (1 MPa/°C) and on FBG in the SMF (2.3 MPa/°C) (Wu C et al., 2010).

To test the system response to the RI change, the fiber device was fixed on a translation stage, and immersed by concentrations of salt water and the reflection spectra recorded had a resolution of 0.05 nm. Each time after the liquid sample was measured, the fiber sensor head was rinsed with methanol carefully until the original spectrum (i.e., the reference spectrum) could be restored and no residue liquid was left on the sensor head surface. Fig. 8 shows the interference fringe dip wavelength shift with the RI change and the sensitivity of ~73.54 nm/RIU was achieved. In the inset of Fig. 8, the wavelength variation as a function of RI is plotted.

Currently, the pressure measurement range achieved in the experiment is limited by the air pump used, which only provides a pressure value up to 1 MPa. However, our device has the potential of achieving much higher pressure measurement range due to its robust structure. As a number of wavelength dips exist in the reflection spectrum as shown in Fig. 3(a), and the device is sensitive to a range of physical parameters, a simultaneous multiple parameter measurement can be expected.

4 CONCLUSIONS

In summary, we demonstrated and fabricated an optical fiber FP interferometer which is composed of etched MMF filled with UV adhesive. The gas pressure change induces the air-cavity length change, which causes the change in optical path difference of the MZI, and in turn leads to the reflection spectrum shift. The sensor device exhibits a high pressure sensitivity of -40.94nm/MPa and a good temperature sensitivity of 213 pm/°C within the range from 55°C to 85°C, and a RI sensitivity of ~-73.54 nm/RIU within the range from 1.332 to 1.372. The temperature cross-sensitivity of the device is 5.2kPa/°C. Such a device is based on low cost MMF, compact in size, robust in structure, simple in fabrication, convenient in operation, which makes it highly attractive for pressure sensing.

ACKNOWLEDGMENTS

REFERENCES

Roriz P., et al., 2013. Review of fiber-optic pressure sensors for biomedical and biomechanical applications[J]. *Journal of biomedical optics, 18(5): 050903-050903.*

Pevec S. and Donlagic D., 2012. Miniature all-fiber Fabry–Perot sensor for simultaneous measurement of pressure and temperature[J]. *Applied optics, 51(19): 4536-4541.*

Guo F., et al., 2012. High-sensitivity, high-frequency extrinsic Fabry–Perot interferometric fiber-tip sensor based on a thin silver diaphragm[J]. *Optics letters, 37(9): 1505-1507.*

Xu F., et al., 2012. High-sensitivity Fabry–Perot interferometric pressure sensor based on a nanothick silver diaphragm[J]. *Optics letters, 37(2): 133-135.*

Ma J., et al., 2012. High-sensitivity fiber-tip pressure sensor with graphene diaphragm[J]. *Optics letters, 37(13): 2493-2495.*

Jin L., et al., 2013. Sensitivity characteristics of Fabry-Perot pressure sensors based on hollow-core microstructured fibers[J]. *Journal of Lightwave Technology, 31(15): 2526-2532.*

Eom J., et al., 2015. Fiber optic Fabry–Perot pressure sensor based on lensed fiber and polymeric diaphragm[J]. *Sensors and Actuators A: Physical, 225: 25-32.*

Ran Z., et al., 2015. Novel High-Temperature Fiber-Optic Pressure Sensor Based on Etched PCF FP Interferometer Micromachined by a 157-nm Laser[J]. *IEEE Sensors Journal, 15(7): 3955-3958.*

Hou M., et al., 2014. Sensitivity-enhanced pressure sensor with hollow-core photonic crystal fiber[J]. *Journal of Lightwave Technology, 32(23): 4035-4039.*

Yuan W., et al., 2011 Note: Optical fiber milled by focused ion beam and its application for Fabry-Pérot refractive index sensor[J]. *Review of Scientific Instruments, 82(7): 076103.*

Coelho L., et al., 2012. Simultaneous measurement of partial pressure of O_2 and CO_2 with a hybrid interferometer[J]. *Optics letters, 37(15): 3063-3065.*

Hu G. and Chen D., 2012. Side-hole dual-core photonic crystal fiber for hydrostatic pressure sensing[J]. *Journal of Lightwave Technology, 30(14): 2382-2387.*

Liu Z., et al., 2012. Intermodal coupling of supermodes in a twin-core photonic crystal fiber and its application as a pressure sensor[J]. *Optics express, 20(19): 21749-21757.*

Wu C., et al., 2010. Characterization of pressure response of Bragg gratings in grapefruit microstructured fibers[J]. *Journal of Lightwave Technology, 28(9): 1392-1397.*

Xu B., et al., 2015. Fiber-tip gas pressure sensor based on dual capillaries[J]. *Optics express, 23(18): 23484-23492.*
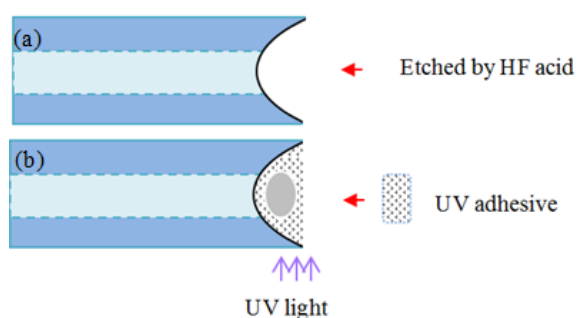
APPENDIX

Figure 1: Schematic diagram of the fabrication process of the optical fiber sensor head. (a) A taper-shaped hole at the end of MMF is formed by HF etching. (b) The taper-shaped hole at the end of MMF is filled by UV adhesive.
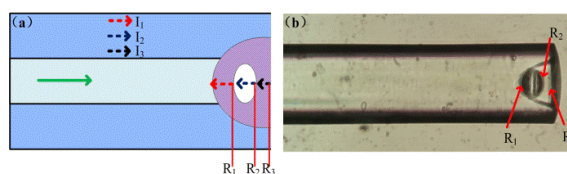

Figure 2: (a) Schematic diagram and (b) the microscope image of the sensor head.
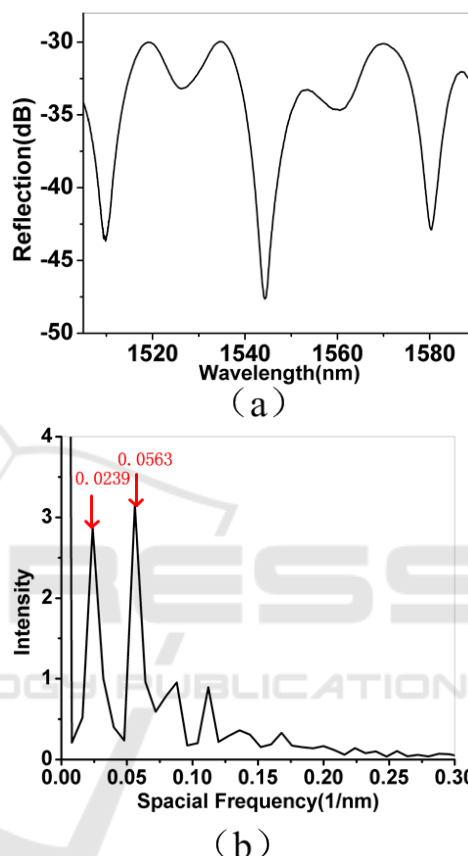

Figure 3: (a) Reflection spectra of the device sample. (b) Spatial frequency spectra of the device sample.
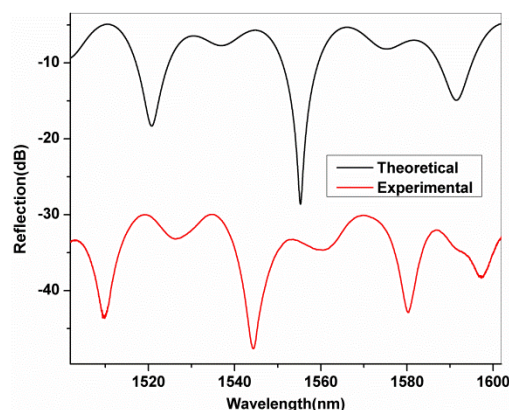

Figure 4: Reflection spectra of the FP cavity device obtained from theoretical simulations and experiment.
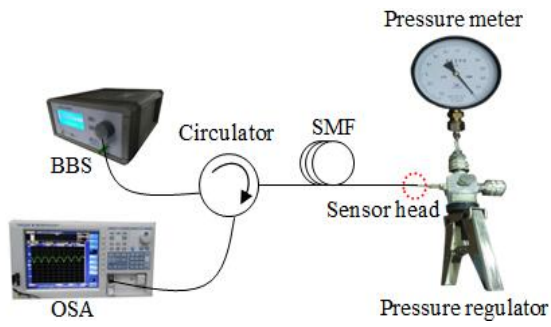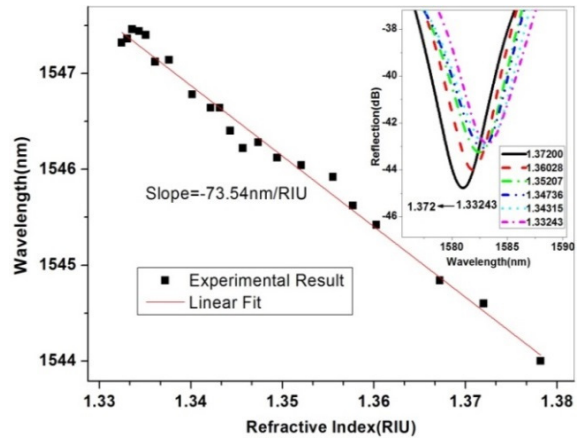
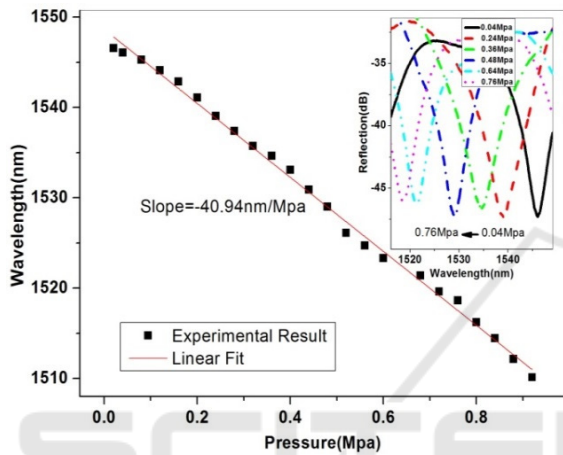Figure 5: Schematic diagram of experimental setup.

Figure 6: Dip wavelength shift with the increase of pressure, and the inset shows the reflection spectra of the device at different pressures.
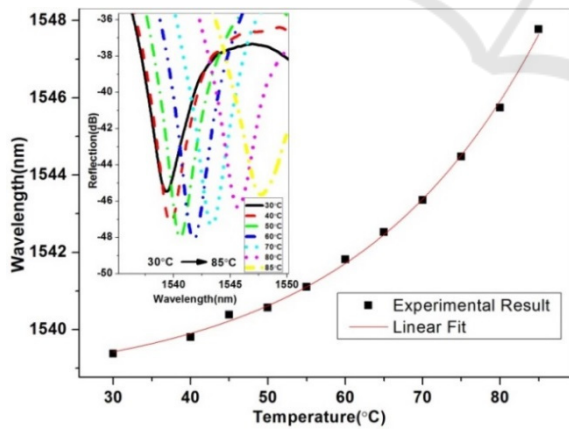

Figure 7: Fringe dip wavelength shift with the temperature variation. Inset shows the reflection spectra of the device at different temperatures.

Figure 8: Dip wavelength shift with RI, and the inset shows the reflection spectra of the device at different RI values.